

Article

Role of *Scirpus mariqueter* on Methane Emission from an Intertidal Saltmarsh of Yangtze Estuary

Yangjie Li ^{1,2}, Dongqi Wang ^{2,*} , Zhenlou Chen ², Haiyan Jin ¹, Hong Hu ², Jianfang Chen ¹ and Zhi Yang ¹

¹ Key Laboratory of Marine Ecosystem and Biogeochemistry of State Ocean Administration, Second Institute of Oceanography, State Ocean Administration, Hangzhou 310012, China; liyangjie@sio.org.cn (Y.L.); jinhaiyan@sio.org.cn (H.J.); jfchen@sio.org.cn (J.C.); yangz@sio.org.cn (Z.Y.)

² School of Geographic Sciences, East China Normal University, Shanghai 200241, China; zlchen@geo.ecnu.edu.cn (Z.C.); dhu_hong@126.com (H.H.)

* Correspondence: dqwang@geo.ecnu.edu.cn; Tel.: +86-21-6223-3333

Received: 25 December 2017; Accepted: 4 April 2018; Published: 10 April 2018



Abstract: The role of wetland plant (*Scirpus mariqueter*) on methane (CH₄) emissions from a subtropical tidal saltmarsh of Yangtze estuary was investigated over a year. Monthly CH₄ flux and pore-water CH₄ concentration were characterized using static closed chamber technique and pore-water extraction. Measured chamber CH₄ fluxes indicated that saltmarsh of the Yangtze estuary acted as a net source of atmospheric CH₄ with annual average flux of 24.0 mgCH₄·m⁻²·day⁻¹. The maximum chamber CH₄ flux was in August (91.2 mgCH₄·m⁻²·day⁻¹), whereas the minimum was observed in March (2.30 mgCH₄·m⁻²·day⁻¹). Calculated diffusion CH₄ fluxes were generally less than 6% of the chamber fluxes. Significant correlations were observed between the chamber CH₄ flux and rhizospheric pore-water CH₄ concentration (11–15 cm: $p < 0.05$, $R = 0.732$; 16–20 cm: $p < 0.05$, $R = 0.777$). In addition, chamber CH₄ fluxes from July to September constituted more than 80% of the total annual emission and were closely correlated with aboveground biomass yield of *S. mariqueter*. The results indicated that *S. mariqueter* transportation was the dominant CH₄ emission pathway and it provided an efficient route for the belowground CH₄ to escape into the atmosphere while avoiding oxidation, leading to CH₄ emissions.

Keywords: estuarine salt marsh; vascular plant; carbon cycles; methane emission

1. Introduction

Methane (CH₄) is the second most important greenhouse gas in the atmosphere [1]. One of important pathways of CH₄ formation is through fermentation mediated by microbiological process and controlled by oxygen availability and the amount of labile organic matter [2]. Another CH₄ formation pathway is carbonate reduction, which is believed to be a main process of CH₄ production in marine systems [3]. As CH₄ exchange at air–soil boundary layer is determined by its net result of production and consumption, CH₄ emissions at ecosystem level cannot be accurately quantified without accounting for the potential of CH₄ oxidation [4–6]. It has been reported that most of the CH₄ formed in the anoxic environment is biologically oxidized to CO₂ before escaping out of the sediments [7,8]. In wetland sediments, CH₄ oxidation mediated by methanotrophs could occur in both aerobic and anaerobic conditions [9–11].

There are three pathways for dissolved CH₄ in sediment pore-water to reach the atmosphere: molecular diffusion, bubble ebullition, and vascular plant transport [12,13]. High belowground CH₄ stock resulted from rapid microbial CH₄ production creates concentration gradients at air–soil boundary layers [14], which drives CH₄ diffusion following the Fick's first law [15]. In some cases,

the diffusion fluxes were found to be smaller than bubble ebullition and vascular plants transport [16]. To adapt to long-term water flooding, wetland plants develop aerenchyma as a pathway for internal gas transport. This pathway is bidirectional such that oxygen can be transported belowground tissues and CH₄ be vented to the atmosphere [17]. Wetland plants can also greatly influence CH₄ production and consumption by secreting O₂ and exudates in rhizosphere [18–20]. In addition, the plant transportation of CH₄ could play an important role in CH₄ emissions [14]. This is especially true in vegetated wetlands where plant transportation usually acts as the main emission pattern of CH₄ [20,21], even though the magnitude of CH₄ emissions may vary significantly among different species [20,22–24].

The Yangtze estuary, located in the subtropical area with a clear four seasons, is one of the biggest estuaries in the world. Annually, the Yangtze River transports 4.80×10^8 tons of sediment to the East China Sea, and about half of that settles in the estuary, thereby forming an extensive intertidal zone [25]. Thus, intertidal marshes in Yangtze estuary may play an important role in carbon cycles including both carbon sequestration and release in the regional scale. Previously, Wang et al. [26] reported the CH₄ emission fluxes and seasonal influence in this area. Bu et al. [27] studied the semi-lunar tidal cycling on sediment CH₄ emissions. Yin et al. [28] revealed the influences of *Spartina alterniflora* invasions on both CH₄ and N₂O fluxes from the salt marsh, just north of Yangtze estuary. However, few studies focused on the influence of the endemic plant (*S. mariqueter*) on CH₄ emissions in Yangtze estuary. Clarification of the relative contribution of two emission pathways, molecular diffusion and plant transport, would be very useful to reveal the plants' contribution to CH₄ emissions. Besides, Yangtze estuary is also faced with the invasion of the exotic *Spartina alterniflora*, which could greatly decrease the plant density of *S. mariqueter*, thus changing the CH₄ emissions. Therefore, the objectives of this case study were: (1) to elucidate the role of *S. mariqueter* on methane emission; (2) to identify the seasonal CH₄ emission patterns; and (3) to examine the relationship between CH₄ emissions and pore-water CH₄ concentrations, at representative point of an intertidal saltmarsh at Yangtze estuary.

2. Methods and Materials

2.1. Study Site

Yangtze estuarine wetlands continue extending to East China Sea rapidly because of the abundant sediment import from the upper reaches [25]. Dongtan in the east Chongming Island is the largest and most conserved intertidal wetland in Yangtze estuary, which is about 100 km² and composed of saltmarsh and bare flat. The shape of saltmarsh is semilunar, and the widest middle part is about 4 km (Figure 1). Research and sampling point is selected at about the center of the saltmarsh (31°30.111' N, 121°59.024' E). The point is not submerged during the neap tide and submerged for several hours during the spring tide. Sampling was carried out at low tide. *Phragmites*, *S. mariqueter* and the invasive *Spartina alterniflora* compose the vegetation community of saltmarshes. *S. mariqueter* is the native species in Yangtze estuary. In general, one axillary bud per corm sprouts to form a new shoot at the depth of 20 cm in spring, which determines that most of the roots distribute within the depth of 20 cm [29]. At the base of the new shoot, constituted by a corm, usually one to three rhizomes develop and form new shoots [30]. The growing season for *S. mariqueter* generally occurs from late April to early November with the most active growth occurring during the three summer months (July, August and September), and it dies off at the end of the growing season and they gradually fall over. Along with the continuous sediment deposition, the dead plant will be buried by the sediment and they cannot be flow out with the tide due to the deeper root fixation [31].

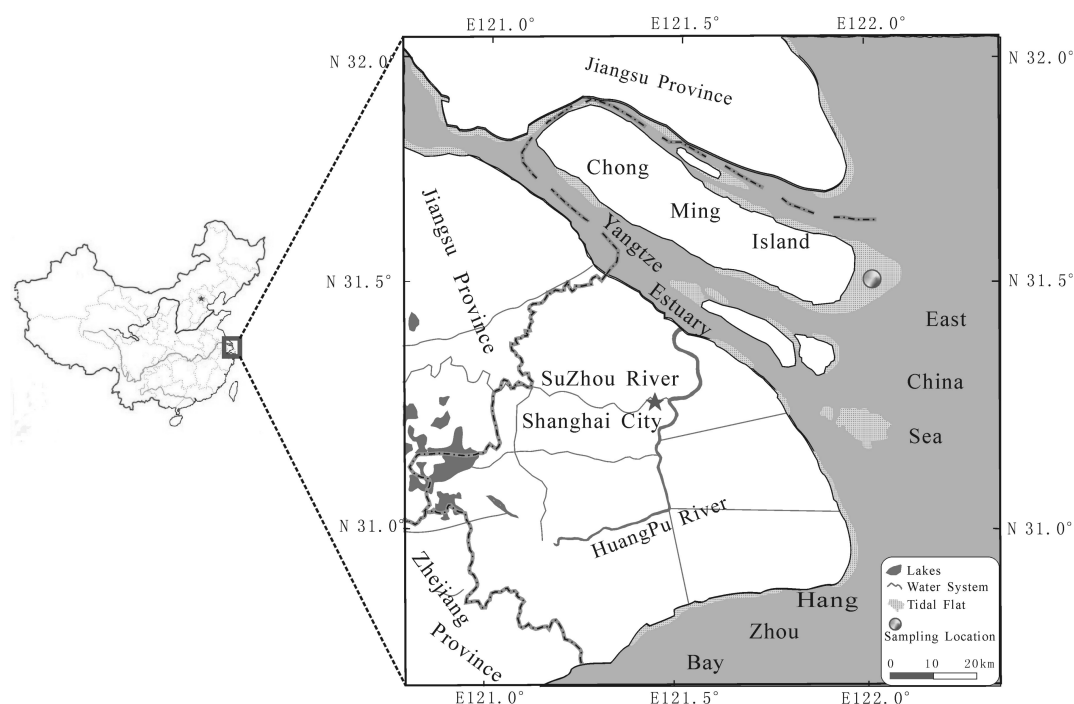


Figure 1. The sampling site in Yangtze estuary. The studied salt marsh was mainly dominated by the endemic species of *S. mariqueter*.

2.2. Sampling

A sediment core (60-cm long) was collected monthly from April to December 2011 using a PVC pipe (inner diameter: 12 cm, length: 100 cm). Core sampling was not carried out from January to March because the preparatory work was not being done during that period. The core was sealed with tapes and carried back to the laboratory for the measurement of pore-water CH_4 concentration within one day.

Static closed chamber technique was adopted to measure CH_4 fluxes 70 times from February to December 2011. Three stainless-steel collars were inserted into the soil to a depth of 5 cm including one bunch of moderate growth size of *Scirpus mariqueter*, half hour before gas sampling, and, then, triplicate transparent chambers made of 3-mm thickness Perspex cylinder were placed on collars, and an airtight closure was ensured by water sealing during the measurements. Considering that the vegetation height, even during the peak of the growing season, was no more than 50 cm, the dimensions of the chambers are 50-cm height and 30-cm inner diameter. Small electric fans and kerosene thermometers were fixed inside the chambers for the air blending in the chambers and the temperature measurement inside the chambers. For each chamber, a venting tube (5 mm inner diameter and 18.8 m long) was used to balance the air pressure between inside and outside chambers [32], and a polyethylene pipe connected with a three-way stopcock was fixed on the chamber top for sampling. All the connections and gaps were sealed by silicone gel to ensure chambers were air tight. Immediately after installing each chamber and again 30 min later, 180 mL gas sample was drawn out by using a syringe with a three-way airtight stopcock and injected into a pre-vacuumed air bag (plastic bag plated with Aluminum inside), which is inert to the greenhouse gas. Gas samples were carried back to the laboratory and analyzed for CH_4 .

Environmental factors including light intensity, air temperature and sediment temperature at different depths (5 cm, 10 cm and 15 cm) were recorded synchronously using a TES-1332 photometer, spirit thermometer and geothermometer at each time of gas sampling. The aboveground biomass of *S. mariqueter* was measured monthly from April to December. Vegetation samples were collected from seven 50 cm \times 50 cm randomly selected quadrats, maintaining approximately 3–5 m spacing between

quadrats. In each quadrat, the aboveground vegetation was cut carefully, then the number of living shoots were counted, and the shoot weight and cross-section area were measured and recorded.

2.3. Pore-Water CH₄ Extraction

The pore-water CH₄ concentration was measured in the laboratory based on static headspace method within one day after the core was sampled. Fifty milliliters of distilled water were transported into a headspace tube equipped with a screws cap which has a hole and silicone septum. The 60-cm long sediment cores were sliced at 1-cm interval, and then 10 mL of the subsamples in each layer were put into the prepared headspace tube quickly. The tube was capped with the silicone septum immediately and set on a shaker for 20 min at 150 rpm to make the sediment fully blend with the aerated distilled water forming slurry and gas equilibrium between slurry and headspace air. After 20 min of shaking, 10 mL gas sample was extracted with a 50 mL syringe from the headspace of each tube for CH₄ concentration measurement.

2.4. Sediment Properties

The CH₄ in samples was measured using an Agilent 7890A Gas Chromatography (GC) equipped with a FID detector. Sediment water content was calculated based on the mass method. The wet and dry weight of the sediment samples were separately measured before and after they were freeze-dried with a freeze dryer (CHRIST ALPHA 4-1/LD plus). Dried sediment samples were ground and sieved to analyze sediment organic carbon (SOC) based on K₂Cr₂O₇-H₂SO₄ oxidation method [33]. The sediment water content (SWC) was obtained by using the difference between the wet and dry weights. Average particle size (APS) and medium diameter (MD) are measured by laser granularity meter (Coulter LS13320). Extractable nitrogen (NO₃⁻-N and NH₄⁺-N) was determined by extracting 10 g of dry sediment sample with 2 mol·L⁻¹ KCl followed by detection of NO₃⁻-N using a continuous flow analyzer (FUTURA, Alliance Co.), and NH₄⁺-N based on standard colorimetric method [34]. For acid volatile sulfide (AVS) measurement, approximately 2 g of sediment were added to the reaction flask and sparged for 2 min with pure N₂ (120 cm³·min⁻¹). The sulfide in the sediment was liberated by extraction with 1 mol·L⁻¹ HCl for 40 min at room temperature and then trapped in a solution of 0.2 mol·L⁻¹ (CH₃COO)₂Zn and 0.1 mol·L⁻¹ CH₃COONa with a continuous N₂ flow to form ZnS. Each trap was quantified using the methylene blue method [35,36].

2.5. Data Calculating

Chamber flux was calculated based on the following equation:

$$F = \frac{\Delta c}{\Delta t} \cdot \frac{V}{A} \quad (1)$$

F is the CH₄ fluxes at the sediment–air interface (mgCH₄·m⁻²·h⁻¹), V is the chamber volume(m³), A is the sediment area in the base of sampling chamber(m²), $\frac{\Delta c}{\Delta t}$ is the change of CH₄ concentration with time (mgCH₄·L⁻¹·h⁻¹), $c = \frac{P}{RT} \times m$ (mgCH₄·L⁻¹), P is the atmospheric pressure in sampling field, R is the gas constant (8.314 J·mol⁻¹·K⁻¹), T is the temperature (Kelvin Temperature, K), and m is the molar mass of the gas molecule.

Pore-water CH₄ concentration was calculated by the following equation:

$$C = \frac{(C_{AIR} - C_{BLANK}) \times V_{AIR} + (C_{AIR} - C_{BLANK}) \times \alpha \times V_{WATER}}{V_{POREWATER}} \quad (2)$$

C is the CH₄ concentration in pore-water (mgCH₄·L⁻¹), C_{AIR} is the measured CH₄ concentration in the headspace of tubes (mgCH₄·L⁻¹), V_{AIR} is the volume of the headspace of tubes (L), and α is the Bunsen coefficient. V_{WATER} is the total volume of aerated distilled water in tubes and the pore water in

sediment samples (L). $V_{POREWATER}$ is the volume of the pore water of the sediment sample (L). C_{BLANK} is the measured CH_4 concentration of the pure water ($\text{mgCH}_4 \cdot \text{L}^{-1}$).

Diffusive fluxes of CH_4 were calculated from linear pore-water concentration gradients according to Fick's first law assuming steady state conditions. The diffusion equation is described as Equation (3):

$$F_{cal} = D_S \frac{\Delta C}{\Delta Z} = D_S \frac{C_S - C_A}{\Delta Z} \quad (3)$$

where F_{cal} is the calculated diffusion CH_4 flux ($\mu\text{molCH}_4 \cdot \text{cm}^{-2} \cdot \text{s}^{-1}$), $\frac{\Delta C}{\Delta Z}$ represents the CH_4 concentration change with sediment depth ($\mu\text{molCH}_4 \cdot \text{cm}^{-3} \cdot \text{cm}^{-1}$), ΔZ is the diffusion distance (cm), C_S is measured CH_4 concentration in the surface sediment pore water ($\mu\text{molCH}_4 \cdot \text{cm}^{-3}$), C_A is the saturation concentration of dissolved CH_4 in ambient air ($\mu\text{molCH}_4 \cdot \text{cm}^{-3}$), and D_S is the effective diffusion coefficient for CH_4 in sediment pore-water. D_S is calculated by the polynomial regression equation obtained by the measured diffusion coefficients for CH_4 in water (D_w) in the range 0 °C to 35 °C ($\text{cm}^2 \cdot \text{s}^{-1}$) (83rd Edition of the Handbook of Physics and Chemistry) which yielded the relationship [37]:

$$D_w = 8.889 \times 10^{-11} T^3 - 1.714 \times 10^{-9} T^2 + 3.721 \times 10^{-7} T + 8.771 \times 10^{-6} \quad (4)$$

and then porosity corrected by Equation (5) from Lerman [38]:

$$D_S = D_w \times \phi^2 \quad (5)$$

where ϕ is sediment porosity. To make the calculated diffusion flux be consistent with the total emission flux, F_{cal} was finally expressed in $\text{mgCH}_4 \cdot \text{m}^{-2} \cdot \text{day}^{-1}$.

2.6. Statistical Analysis

The total CH_4 fluxes were presented as means of the replications. SPSS (Version 17.0) was used to perform all of the statistical data tests. Pearson correlation analyses were used to examine the relationship between fluxes and the measured environmental variables. The statistical results were regarded as significant if the P values were lower than 0.05 or 0.01.

3. Results

3.1. Environmental Factors

Table 1 shows seasonal climatic, vegetation and soil physiochemical parameters of experimental site. Air temperature exhibited significant seasonal variation with the highest and lowest temperatures in July and February, respectively. Highest biomass of *S. maritima* occurred in August ($692.6 \text{ g} \cdot \text{m}^{-2}$). The number of living shoots increased with the biomass and also reached the highest value in August. Since then, the plant began to wither and almost all of them fell over on the sediment surface in December. SOC did not show substantial changes throughout the year. SWC stayed at a relatively low level from February to April but increased in the following months. APS and MD indicated that sediment was dominated by silt fractions. In terms of the extractable nitrogen, NH_4^+ -N content was generally higher than that of NO_3^- -N, which probably indicated that the tidal marsh was generally under denitrification condition rather than nitrification. On the other hand, the irregular variation of AVS content throughout the year suggested that the redox potential of the microenvironment may differ a lot in this estuarine system (Table 1). AVS is mainly produced by the sulfate reduction process which occurred after the O_2 and NO_3^- were utilized. Thus, AVS can be seen as an index of the sediment redox condition. Monthly AVS distribution in the sediment profile is shown in Figure 2, which indicated that the AVS in the surface sediment is usually lower than the deeper sediment. Besides, the AVS showed complex variation along with depth and month.

Table 1. Climatic, plant and soil physiochemical parameters of experimental site.

Month	Temperature (°C)					PAR (W·m ⁻²)	Biomass		SOC (g·dm ⁻³)	SWC (%)	APS/MD (µm)	NH ₄ ⁺ -N (mg·kg ⁻¹)	NO ₃ ⁻ -N (mg·kg ⁻¹)	AVS (µg·g ⁻¹)
	AAT	ATR	GT5	GT10	GT15		(g·dm·m ⁻²)	Number of Living Shoots in 50 cm × 50 cm Quadrats						
February	4	-2.0~9.0	3	2	1	8~266	-	-	7.27	43	16.81/23.81	3.04	0.15	-
March	12	7.5~14.5	10	9	9	17~233	-	-	6.91	39	15.06/20.23	4.88	0.19	7.46
April	25	16.0~28.0	20	20	17	15~304	44.6	66	7.59	36	14.31/20.07	7.54	0.12	1.37
May	23	15.5~29.5	23	21	20	35~317	105.9	223	6.78	55	12.51/16.86	4.82	0.98	14.3
June	27	25.0~28.5	26	26	26	30~145	433.9	403	7.86	54	7.747/9.527	5.65	0.49	6.35
July	33	30.0~35.5	31	32	29	38~297	364.1	445	8.42	66	7.129/8.744	4.33	ND	8.28
August	25	23.5~26.0	25	25	25	15~98	692.6	972	7.12	91	6.636/7.891	4.98	0.59	3.43
September	20	16.0~25.0	25	24	23	38~313	534.1	869	7.65	46	7.402/9.479	4.48	0.49	11.5
October	22	16.0~24.0	21	21	20	24~284	263.9	623	8.01	55	8.317/10.81	4.06	0.10	7.32
November	11	5.5~14.0	14	14	14	19~222	-	-	7.78	69	8.082/10.28	5.25	0.16	12.5
December	7	-1.0~9.5.0	7	6	6	8~188	130.3	-	7.63	65	9.096/11.92	4.07	0.20	-

AAT: average air temperature; ATR: Air temperature range during the sampling day; GT5: Sediment temperature at the depth of 5 cm; GT10: Sediment temperature at the depth of 10 cm; GT15: Sediment temperature at the depth of 15 cm) are the mean value of the daily variation. PAR (Photosynthetically Active Radiation) is shown as the variation range of the daily continuous observations. SOC is the average soil organic carbon values of the surface 25 cm sediments. The rest of the sediment parameters (SWC, APS, MD, NH₄⁺-N, NO₃⁻-N and AVS) are the values of the surface 1 cm sediment.

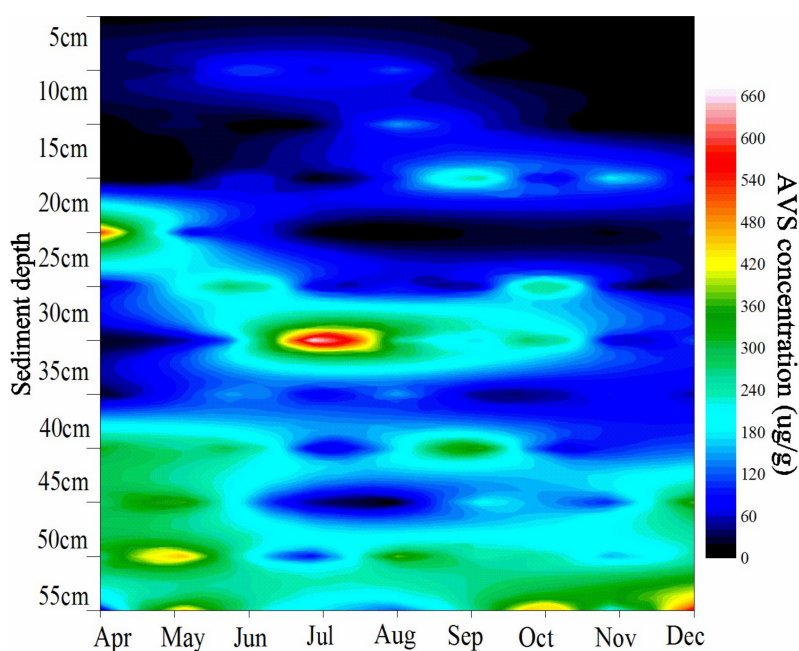


Figure 2. AVS distribution in the sediment profile.

3.2. CH₄ Fluxes

Measured chamber CH₄ fluxes showed a significant seasonal variation throughout the year with the highest ($91.2 \text{ mgCH}_4 \cdot \text{m}^{-2} \cdot \text{day}^{-1}$) and lowest ($2.30 \text{ mgCH}_4 \cdot \text{m}^{-2} \cdot \text{day}^{-1}$) in August and March, respectively (Figure 3). The annual average chamber CH₄ flux in the salt marsh was $24.0 \text{ mgCH}_4 \cdot \text{m}^{-2} \cdot \text{day}^{-1}$. The chamber CH₄ flux did not increase significantly until June when the biomass of *S. mariqueter* rather than temperature increased significantly, and the chamber CH₄ flux was significantly positively correlated with the aboveground biomass ($p = 0.001$, $R = 0.928$) (Figure 4). Chamber CH₄ flux during summer (July, August and September) constituted more than 80% of the total annual emission.

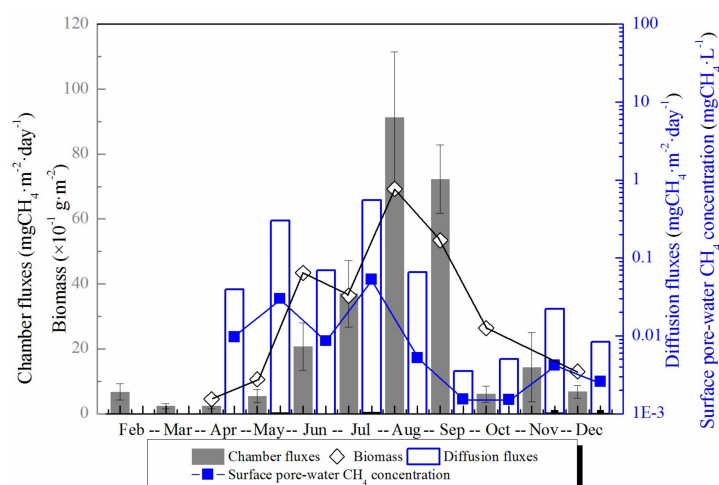


Figure 3. The total chamber CH₄ fluxes, calculated diffusion CH₄ fluxes, the top 1 cm pore-water CH₄ concentration and the biomass of *S. mariqueter* in each month during the year. CH₄ fluxes are presented as column graphs, while the pore-water CH₄ concentration and biomass are presented as line and symbol graphs. The black graphs in the figure are integrated with the left black Y axis and the blue graphs are integrated with the right blue Y axis.

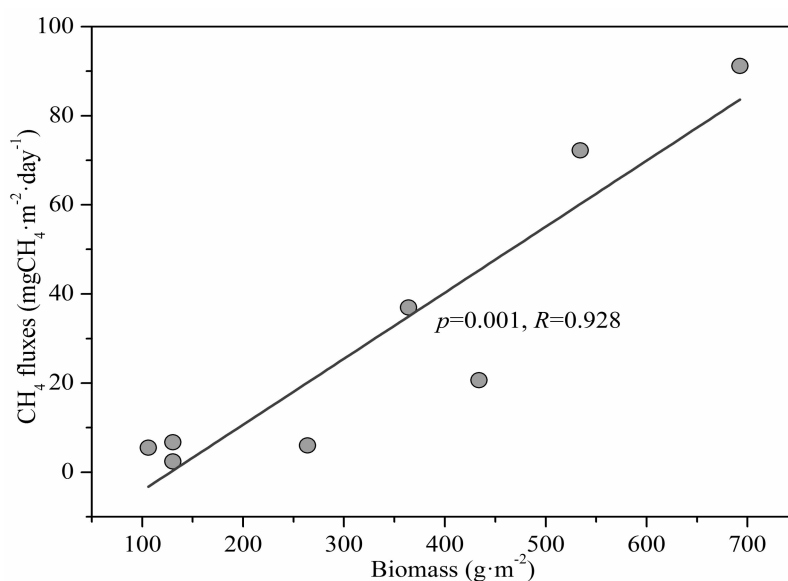


Figure 4. Correlation relationship between the CH_4 fluxes and the aboveground biomass of *S. mariqueter*.

Calculated diffusion CH_4 fluxes between the top 1 cm sediment and air were very low ($<0.55 \text{ mgCH}_4 \cdot \text{m}^{-2} \cdot \text{day}^{-1}$) due to the low pore-water CH_4 concentration in surface sediment (Figure 3). There was evident seasonal variation of diffusion CH_4 fluxes with the highest ($0.55 \text{ mgCH}_4 \cdot \text{m}^{-2} \cdot \text{day}^{-1}$) and lowest ($0.0035 \text{ mgCH}_4 \cdot \text{m}^{-2} \cdot \text{day}^{-1}$) diffusion flux in July and September, respectively (Figure 3). Overall, gas molecular diffusion method contributed a little to the total CH_4 emission with the highest proportion of 5.53% in May.

In addition, regression analysis of different temperatures (air temperature and the sediment temperature at different depths 5 cm, 10 cm and 15 cm) and chamber CH_4 fluxes revealed that CH_4 fluxes were best fitted with the temperature at the sediment depth of 15 cm where the roots of *S. mariqueter* were concentrated (Figure 5).

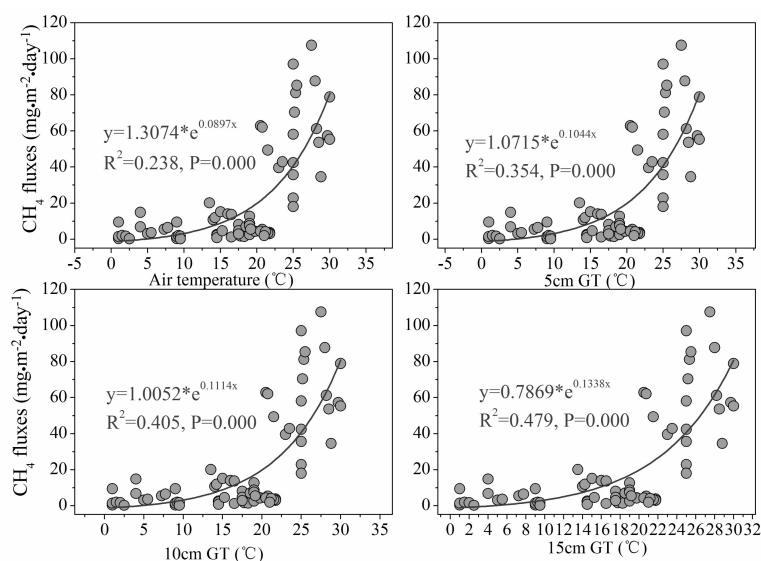


Figure 5. Relationship between chamber CH_4 fluxes and temperature. Abbreviations: 5 cm GT, 10 cm GT and 15 cm GT represent the sediment temperature at depths of 5 cm, 10 cm and 15 cm, respectively ($n = 70$).

3.3. Pore-Water CH₄ Concentration

Top 1 cm pore-water CH₄ concentration did not show any apparent seasonal variation. It was higher in the first half year and decreased to a lower value in the second half year (see Figure 3). Pore-water CH₄ concentration in the top 1 cm was much lower than in the deeper layer sediment, resulting in a low diffusion flux. In the vertical profile, CH₄ concentration increased significantly with depth. Although the pore-water CH₄ concentration in deep sediment layers did not exhibit an apparent synchronously monthly variation with temperature, it did show an evident seasonal change (Figure 6). Pore-water CH₄ concentration of deep sediment layer increased from May to July, decreased through October, and then reached the highest concentration (8.30 mgCH₄·L⁻¹) in November. After that, deep layer sediment pore-water CH₄ concentration decreased again until the next April (Figure 6).

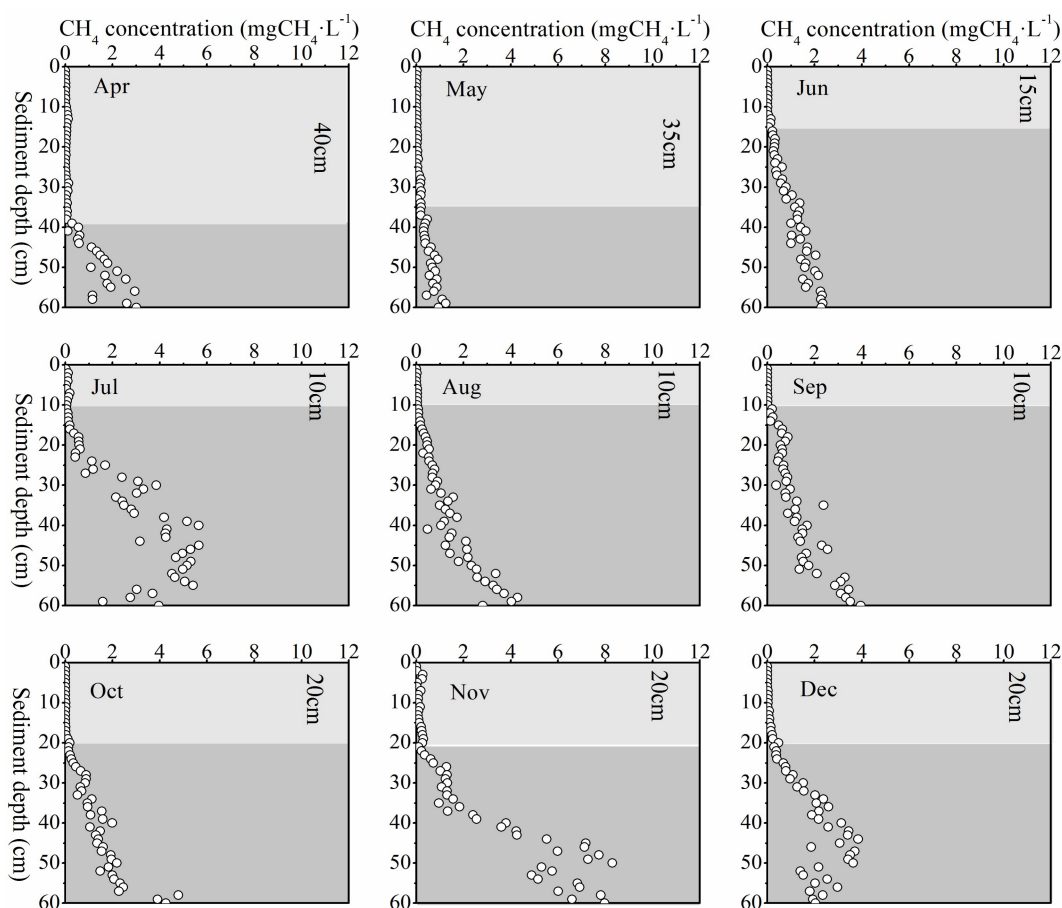


Figure 6. Monthly variation of pore-water CH₄ concentration. A steep increase in pore-water CH₄ concentration occurred when it exceeded 0.1 mgCH₄·L⁻¹ for each month. The light color located above the depth of this steep increase indicates the low CH₄ concentrations, while the dark color indicates the high CH₄ concentrations.

Along with the deep pore-water CH₄ concentration variation, the depth of the steepest increase in CH₄ concentration fluctuated up and down regularly during the year. The transition point of CH₄ concentration increment usually occurred after the concentration exceeding 0.1 mgCH₄·L⁻¹. The location of this interface moved up from April to July and consistently stayed at about 10 cm depth through September, and then it went down from October to November (Figure 6).

Relationship between the pore-water CH₄ concentration and total CH₄ fluxes were also analyzed through Pearson correlation analysis. Significant correlations were observed between CH₄ flux and

pore-water CH₄ concentration only at the depths of 11–15 cm ($p < 0.05$, $R = 0.732$) and 16–20 cm ($p < 0.05$, $R = 0.777$). (see Table 2).

Table 2. Correlation relationships between monthly methane (CH₄) fluxes and the pore-water CH₄ concentration at the different depths ^a, * $p < 0.05$.

Depth	CH ₄ Fluxes ^b	Depth	CH ₄ Fluxes	Depth	CH ₄ Fluxes
0–5 cm	−0.084	21–25 cm	0.590	41–45 cm	−0.034
6–10 cm	0.146	26–30 cm	0.192	46–50 cm	−0.065
11–15 cm	0.732 *	31–35 cm	0.279	51–55 cm	0.219
16–20 cm	0.777 *	36–40 cm	0.101	56–60 cm	0.190

^a The pore-water CH₄ concentration was measured at 1-cm interval, but the mean of the pore-water CH₄ concentrations at 5-cm interval was used to analyze the correlation relationship between the CH₄ fluxes and the underground CH₄ concentrations at different depths of each month. ^b The correlation coefficient “R” for CH₄ fluxes and the averaged pore-water CH₄ concentrations in different depths.

4. Discussion

4.1. Dominant Mechanism of CH₄ Emission

Different types of wetlands may be dominated by different CH₄ emission patterns (plant mediated emission, bubble emission and the molecule diffusion) [39–41]. Anaerobic conditions in wetlands are favorable for CH₄ production and accumulation, which finally create a CH₄ concentration gradient between the underground and atmosphere [42]. Molecular diffusion is driven by the concentration gradient following Fick’s first law of diffusion [37]. Based on Fick’s first law, we calculated the molecular diffusive CH₄ flux from the saltmarsh into the atmosphere. In this study, the calculated diffusion fluxes stayed at very low level with the highest diffusion flux of 0.55 mgCH₄·m^{−2}·day^{−1} in July. The proportion of diffusion fluxes accounted for 0.0048–5.53% of total monthly CH₄ emission during the year. The specific reason for the weak diffusion flux is unclear due to the lack of ground water level, wind speed and the tide movement measurements. It is speculated that the wet condition in the saltmarsh is one of the most probable reasons, since it is known that water condition of the media can greatly influence the gas diffusion efficiency [43]. The *S. mariqueter* marsh in Yangtze estuary is located at the lower position of the tidal flat and was regularly submerged by the tide water. Surface sediments are always kept under a wet condition (this can be seen from the surface sediment water content in Table 1), which greatly inhibits the gas diffusion from surface sediment into air. In addition, the surface sediment usually stayed at a relative oxic condition, which can be seen from the low AVS concentrations in the surface sediment. Pore-water CH₄ concentrations was significantly correlated with AVS concentrations ($p < 0.01$, $R^2 = 0.265$). It was also proven in the previous study that oxygen could easily penetrate sediment creating an oxic condition when the sediment surface exposes to the air [44]. Previous studies reported that the existence of oxidizing zones can greatly reduce the diffusion CH₄ flux. According to Yun et al. [45], the aerobic methanotrophs could oxidize more than 90% of the CH₄ produced in the anoxic conditions. Similar results were also obtained by Liebner et al. [46] who found that the diffusive CH₄ flux from the sediment surface only accounted for less than 2% of the total flux into the atmosphere in an alpine fen due to the linearly decreased pore water CH₄ concentration at the depth of 0–15 cm. Our research also indicated that the intense oxidation of surface pore-water CH₄ directly led to the weak diffusive CH₄ flux.

In this study, *S. mariqueter* was found to facilitate CH₄ emissions and the plant emitted more than 94% of the total CH₄, which was consistent with many previous studies (Table 3). The highest chamber CH₄ flux appeared in August when *S. mariqueter* was in the utmost abundant with the biggest aboveground biomass throughout the year of 692.6 g·m^{−2}. The chamber CH₄ fluxes of the three thriving months of *S. mariqueter* (July, August and September) constituted more than 80% of the total annual emission. The chamber CH₄ flux decreased greatly at the end of growing season, which was consistent with the research of Chmura et al. [47]. The aerenchyma of wetland plants had two opposite

effects on CH₄ emission. Negatively, it could transport oxygen downward, creating an aerobic zone in rhizosphere [19]. The enhanced oxygen availability in sediment could inhibit CH₄ production and accelerate CH₄ consumption [46,48]. On the other hand, presence of aerenchyma in wetland plants also provides gas channels for CH₄ escaping from underground to the atmosphere [16,49]. In a previous research of similar salt marsh, the net effect of these two processes was found to change along with the *S. mariqueter* growth stage [26]. It is indicated that the quantity of upward transported CH₄ to the air through *S. mariqueter* exceeded the oxidized CH₄ by downward transported O₂ through *S. mariqueter*.

The fact that chamber CH₄ fluxes were significantly correlated with aboveground biomass of *S. mariqueter* suggested significant effect of marsh plant growth on CH₄ emission. Besides, regression analysis of different temperatures (air temperature and the sediment temperature at different depths 5 cm, 10 cm and 15 cm) and chamber CH₄ fluxes revealed that CH₄ fluxes were best fitted with the temperature at the sediment depth of 15 cm where the roots of *S. mariqueter* were concentrated [29] (Figure 5). This indicates that the rhizospheric temperature would be a good predictor of CH₄ emission. While higher temperature usually leads to stronger methanogenesis and CH₄ accumulation [50], our result emphasizes the significance of the temperature increase in rhizosphere that enhanced the CH₄ emission. These observations further pointed to the great contribution of plant transportation to overall CH₄ emissions in this salt marsh ecosystem. Previous research showed that the wetland plant, no matter living or dead, could provide a continuous escaping route for CH₄ even in winter [51]. Nonetheless, our results indicated that the strongest transportation capacity of CH₄ by individual plant appeared in August with the highest CH₄ flux at 2.34×10^{-2} mgCH₄·stem⁻¹·day⁻¹ in these Yangtze estuary wetlands.

Table 3. Plant contributions of different species to CH₄ emissions.

Vegetation Type	Proportion of Plant Emitted CH ₄ (%) ^a	Plant Treatment ^b	References
<i>C. lasiocarpa</i>	73–82	clipping ^c	[21]
<i>C. meyeriana</i>	75–86	clipping	[21]
Rice	94	clipping	[52]
Rice	97	clipping	[53]
Rice	90	clipping	[54]
Reed	60	clipping	[52]
Weeds	84	clipping	[52]
Sedge	79	uprooting ^d	[55]
<i>Eriophorum latifolium</i>	80	uprooting	[20]
Sedge	94	clipping	[56]
Sedge	83	clipping	[57]
<i>E. vaginatum</i>	88	clipping	[58]

^a The proportion of plant transported CH₄ fluxes in the total CH₄ fluxes. ^b Different approaches to quantify the plants' effects on CH₄ emissions. ^{c,d} The most commonly adopted approaches in studying the plant transportation capacity for CH₄. ^c The plant stems covered by the static closed chamber were clipped leaving the stem section on the sediment surface; ^d Plants covered by the static closed chamber were uprooted.

4.2. The Implication of Pore-Water CH₄ Concentration for CH₄ Emission

Static pore-water CH₄ concentration from the surface to deep sediment was a net result of CH₄ production and consumption, which could be affected by many environmental factors such as the redox potential, sediment organic carbon content, the distribution of methanogens and methanotroph, etc. [59–61]. In this study, the deep pore-water CH₄ concentration did not exhibit synchronously seasonal variation with temperature (Figure 2), which was consistent with previous study in an alpine fen [46]. Sediment pore-water CH₄ concentration profiles showed that there was an interface where the CH₄ concentration steeply increased after it exceeded 0.1 mgCH₄·L⁻¹ (Figure 6). Although the CH₄ concentration in the surface 10 cm sediment did not show apparent seasonal variations, the depth of this interface did vary and was shallower (~10 cm) in summer than in other seasons (Figure 6). Previous studies showed that the surface sediment pore-water CH₄ concentration was influenced by the oxygen concentration easily and more than 90% of the CH₄ produced in anoxic conditions could

be oxidized in the upper aerobic conditions [62]. Conversely, the pore-water CH_4 concentration could be seen as the indicator of environmental oxidation–deoxidation status. In our study, we attributed the upper layer of the sediment where CH_4 concentration was lower than $0.1 \text{ mg CH}_4 \cdot \text{L}^{-1}$ to the active CH_4 oxidization (aerobic and anaerobic). Above this interface, CH_4 concentration was controlled by the aerobic and anaerobic oxidation process and maintained at a low level (Figure 5). Below this interface, CH_4 concentration increased sharply, which was controlled by the anaerobic oxidation and production and diffusion from deeper layer. The effects of temperature on the depth of this “interface” could be explained from two aspects. On the one hand, under high temperature, oxygen penetration into sediment was generally reduced because the solubility of atmospheric oxygen decreased with temperature increase [44]. On the other hand, intensive respiration took place at high temperature, which accelerated the oxygen consumption within the surface sediment zones [63,64].

The analysis of the correlation between chamber CH_4 fluxes and the pore-water CH_4 concentration in different depths showed that only the pore-water CH_4 concentration at the depths of 11–15 cm and 16–20 cm, where the dense roots of *S. mariqueter* are distributed, best predicted the chamber CH_4 fluxes (see Table 2). The increased temperature in summer raised the depth of reactive layer for CH_4 production to the depth of plant root distribution, which directly promoted the rhizospheric CH_4 uptake from sediment pore water and prevented the CH_4 oxidation in diffusion. The positively correlated chamber CH_4 fluxes and rhizospheric CH_4 concentration revealed that overall *S. mariqueter* acted as a promoter of CH_4 emission when taking both rhizospheric CH_4 oxidation and transportation into consideration.

The lack of significant relationship between the surface (0–10 cm) pore-water CH_4 concentration and chamber CH_4 fluxes further indicated the small contribution of gas molecular diffusion to CH_4 emission. Although the pore-water CH_4 concentration was apparently higher in the deeper layers, it had little effect on CH_4 emission, probably because most of the upward diffusive CH_4 was anaerobically oxidized due to the long-distance migration [64,65]. In addition, the CH_4 in the deep sediment scantily contributed little to CH_4 fluxes through bubble emission because the CH_4 concentration was not high enough to form gas bubbles. Previous studies have indicated that bubbles could not form until pore-water CH_4 concentrations exceeded $7.1\text{--}8.0 \text{ mgCH}_4 \cdot \text{L}^{-1}$ [66]. In this research, pore-water CH_4 concentration in surface was only about $0.001\text{--}0.01 \text{ mgCH}_4 \cdot \text{L}^{-1}$, and even the highest pore-water CH_4 concentration in deep sediment layer (below 45 cm) was under $8.0 \text{ mgCH}_4 \cdot \text{L}^{-1}$.

5. Conclusions

This study demonstrated that *S. mariqueter* marsh in Yangtze estuary acted as a net source of atmospheric CH_4 . The annual average chamber CH_4 flux was $24.0 \text{ mgCH}_4 \cdot \text{m}^{-2} \cdot \text{day}^{-1}$ with the peak flux in August when the oxidization layer became shallow (about 10 cm) and the *S. mariqueter* thrived. The calculated diffusion CH_4 fluxes were no more than 6% of the total fluxes, indicating that molecular diffusion was not a major pathway of CH_4 emission in this salt marsh. Analysis of seasonal variation of pore-water CH_4 concentration identified the dominant emission pattern as plant transport, which was evident by significantly positive correlation between CH_4 concentrations in rhizosphere and chamber CH_4 fluxes. In addition, generally low pore-water CH_4 concentration (much less than $8.0 \text{ mg CH}_4 \text{ L}^{-1}$) throughout the year prevented the formation of CH_4 gas bubbles from ebullition. While wetland plant could exert an influence on rhizosphere CH_4 oxidation, the transport function of the plant played a more important role in CH_4 emission in the Yangtze estuary *S. mariqueter* marsh.

Acknowledgments: The authors are deeply indebted to Chu Wang and Huanguang Deng for their assistance with fieldwork and in the laboratory. This work was jointly supported by the National Natural Science Foundation of China (Grant No. 41473094 and No. 41671467), the Ministry of Science and Technology Project Foundation (2014FY210600), the Shanghai Municipal Natural Science Foundation (Grant No. ZR1412100), the research fund from the SKLEC (2015KYYW03), the Natural Science Project of Zhejiang Province (LQ18D060003 and LQ13D060003) and the Scientific Research Fund of the Second Institute of Oceanography, SOA (JG1515).

Author Contributions: Yangjie Li, Dongqi Wang and Zhenlou Chen designed the study; Yangjie Li, Dongqi Wang and Hong Hu performed the fieldwork and laboratory experiment; Yangjie Li wrote the manuscript; Dongqi Wang,

Haiyan Jin and Jianfang Chen helped improve the manuscript before submission; and Dongqi Wang and Zhi Yang helped revise the manuscript according to the reviewers' comments.

Conflicts of Interest: I would like to declare on behalf of my co-authors that the work was original research that has not been published previously, and is not under consideration for publication elsewhere, in whole or in part. All of the listed authors have approved the manuscript.

References

1. IPCC. *Climate Change 2013: The Physical Science Basis*; Cambridge University Press: Cambridge, UK; New York, NY, USA, 2013.
2. Keller, J.K.; Sutton-Grier, A.E.; Bullock, A.L.; Megonigal, J.P. Anaerobic metabolism in tidal freshwater wetlands: I. Plant removal effects on iron reduction and methanogenesis. *Estuaries Coasts* **2013**, *36*, 457–470. [[CrossRef](#)]
3. Whitticar, M.J. Diagenetic relationships of methanogenesis, nutrients, acoustic turbidity, pockmarks and freshwater seepages in Eckernforde Bay. *Mar. Geol.* **2002**, *182*, 29–53. [[CrossRef](#)]
4. Moore, T.R.; Dalva, M. Methane and carbon dioxide exchange potentials of peat soils in aerobic and anaerobic laboratory incubations. *Soil Biol. Biochem.* **1997**, *29*, 1157–1164. [[CrossRef](#)]
5. Segers, R. Methane production and methane consumption: A review of processes underlying wetland methane fluxes. *Biogeochemistry* **1998**, *41*, 23–51. [[CrossRef](#)]
6. Tang, J.; Zhuang, Q.; Shannon, R.D.; White, J.R. Quantifying wetland methane emissions with process-based models of different complexities. *Biogeosciences* **2010**, *7*, 6121–6171. [[CrossRef](#)]
7. Watson, A.; Stephen, K.D.; Nedwell, D.B.; Arah, J.R. Oxidation of methane in peat: Kinetics of CH₄ and O₂ removal and the role of plant roots. *Soil Biol. Biochem.* **1997**, *29*, 1257–1267. [[CrossRef](#)]
8. Fritz, C.; Pancotto, V.A.; Elzenga, J.; Visser, E.J.; Grootjans, A.P.; Pol, A.; Iturraspe, R.; Roelofs, J.G.M.; Smolders, A.J. Zero methane emission bogs: Extreme rhizosphere oxygenation by cushion plants in Patagonia. *New Phytol.* **2011**, *190*, 398–408. [[CrossRef](#)] [[PubMed](#)]
9. Smemo, K.A.; Yavitt, J.B. Anaerobic oxidation of methane: An underappreciated aspect of methane cycling in peatland ecosystems? *Biogeosciences* **2011**, *8*, 779–793. [[CrossRef](#)]
10. Liu, D.Y.; Ding, W.X.; Jia, Z.J.; Cai, Z.C. Relation between methanogenic archaea and methane production potential in selected natural wetland ecosystems across China. *Biogeosciences* **2011**, *8*, 329–338. [[CrossRef](#)]
11. Chowdhury, T.R.; Dick, R.P. Ecology of aerobic methanotrophs in controlling methane fluxes from wetlands. *Appl. Soil Ecol.* **2013**, *65*, 8–22. [[CrossRef](#)]
12. Chanton, J.P. The effect of gas transport on the isotope signature of methane in wetlands. *Org. Geochem.* **2005**, *36*, 753–768. [[CrossRef](#)]
13. Dingemans, B.J.; Bakker, E.S.; Bodelier, P.L. Aquatic herbivores facilitate the emission of methane from wetlands. *Ecology* **2011**, *92*, 1166–1173. [[CrossRef](#)] [[PubMed](#)]
14. Kao-Kniffin, J.; Freyre, D.S.; Balsler, T.C. Methane dynamics across wetland plant species. *Aquat. Bot.* **2010**, *93*, 107–113. [[CrossRef](#)]
15. Lai, D.Y.F. Methane Dynamics in Northern Peatlands: A Review. *Pedosphere* **2009**, *19*, 409–421. [[CrossRef](#)]
16. Belger, L.; Forsberg, B.R.; Melack, J.M. Carbon dioxide and methane emissions from interfluvial wetlands in the upper Negro River basin, Brazil. *Biogeochemistry* **2011**, *105*, 171–183. [[CrossRef](#)]
17. Laanbroek, H.J. Methane emission from natural wetlands: Interplay between emergent macrophytes and soil microbial processes. A mini-review. *Ann. Bot.* **2010**, *105*, 141–153. [[CrossRef](#)] [[PubMed](#)]
18. Larmola, T.; Tuittila, E.S.; Tirola, M.; Nykänen, H.; Martikainen, P.J.; Yrjälä, K.; Tuomivirta, T.; Fritze, H. The role of Sphagnum mosses in the methane cycling of a boreal mire. *Ecology* **2010**, *91*, 2356–2365. [[CrossRef](#)] [[PubMed](#)]
19. Cho, R.; Schroth, M.H.; Zeyer, J. Circadian methane oxidation in the root zone of rice plants. *Biogeochemistry* **2012**, *111*, 317–330. [[CrossRef](#)]
20. Koelbener, A.; Ström, L.; Edwards, P.J.; Venterink, H.O. Plant species from mesotrophic wetlands cause relatively high methane emissions from peat soil. *Plant Soil* **2010**, *326*, 147–158. [[CrossRef](#)]
21. Ding, W.; Cai, Z.; Tsuruta, H. Plant species effects on methane emissions from freshwater marshes. *Atmos. Environ.* **2005**, *39*, 3199–3207. [[CrossRef](#)]
22. Bubier, J.L.; Moore, T.R.; Bellisario, L.; Comer, N.T.; Crill, P.M. Ecological controls on methane emissions from a northern peatland complex in the zone of discontinuous permafrost, Manitoba, Canada. *Glob. Biogeochem. Cycles* **1995**, *9*, 455–470. [[CrossRef](#)]

23. Koh, H.S.; Ochs, C.A.; Yu, K. Hydrologic gradient and vegetation controls on CH₄ and CO₂ fluxes in a spring-fed forested wetland. *Hydrobiologia* **2009**, *630*, 271–286. [[CrossRef](#)]
24. Juszczak, R.; Augustin, J. Exchange of the greenhouse gases methane and nitrous oxide between the atmosphere and a temperate peatland in central Europe. *Wetlands* **2013**, *33*, 895–907. [[CrossRef](#)]
25. Chen, X.; Zong, Y. Coastal erosion along the Changjiang deltaic shoreline, China: History and prospective. *Estuar. Coast. Shelf Sci.* **1998**, *46*, 733–742. [[CrossRef](#)]
26. Wang, D.; Chen, Z.; Xu, S. Methane emission from Yangtze estuarine wetland, China. *J. Geophys. Res.* **2009**, *114*, G02011. [[CrossRef](#)]
27. Bu, N.S.; Qu, J.F.; Zhao, H.; Yan, Q.W.; Zhao, B.; Fan, J.L.; Fang, C.M.; Li, G. Effects of semi-lunar tidal cycling on soil CO₂ and CH₄ emissions: A case study in the Yangtze River estuary, China. *Wetl. Ecol. Manag.* **2015**, *23*, 727–736. [[CrossRef](#)]
28. Yin, S.; An, S.; Deng, Q.; Zhang, J.; Ji, H.; Cheng, X. *Spartina alterniflora* invasions impact CH₄ and N₂O fluxes from a salt marsh in eastern China. *Ecol. Eng.* **2015**, *81*, 192–199. [[CrossRef](#)]
29. Sun, S.; Cai, Y.; An, S. Differences in morphology and biomass allocation of *Scirpus mariqueter* between creekside and inland communities in the Changjiang estuary, China. *Wetlands* **2002**, *22*, 786–793. [[CrossRef](#)]
30. Sun, S.; Gao, X.; Cai, Y. Variations in sexual and asexual reproduction of *Scirpus mariqueter* along an elevational gradient. *Ecol. Res.* **2001**, *16*, 263–274. [[CrossRef](#)]
31. Yu, Z.; Li, Y.; Deng, H.; Wang, D.; Chen, Z.; Xu, S. Effect of *Scirpus mariqueter* on nitrous oxide emissions from a subtropical monsoon estuarine wetland. *J. Geophys. Res.* **2012**, *117*. [[CrossRef](#)]
32. Khalil, M.A.K.; Rasmussen, R.A.; Wang, M.X.; Ren, L. Emissions of trace gases from Chinese rice fields and biogas generators: CH₄, N₂O, CO, CO₂, chlorocarbons, and hydrocarbons. *Chemosphere* **1990**, *20*, 207–226. [[CrossRef](#)]
33. Nelson, D.W.; Sommers, L.E.; Sparks, D.L.; Page, A.L.; Helmke, P.A.; Loeppert, R.H.; Soltanpour, P.N.; Tabatabai, M.A.; Sumner, M.E. Total carbon, organic carbon, and organic matter. In *Methods of Soil Analysis. Part 3—Chemical Methods*; Soil Science Society of America, American Society of Agronomy: Madison, WI, USA, 1996; pp. 961–1010.
34. Grasshoff, K.; Ehrhard, M.; Kremling, K. *Methods of Seawater Analysis*, 2nd ed.; Verlag Chemie: Weinheim, Germany, 1983.
35. Lin, Y.H.; Guo, M.X.; Zhuang, Y. Determination of acid volatilesulfide and simultaneously extracted metals in sediment. *Acta Sci. Circumstantiae* **1997**, *17*, 353–358. (In Chinese)
36. Lee, B.G.; Griscom, S.B.; Lee, J.S.; Choi, H.J.; Koh, C.H.; Luoma, S.N.; Fisher, N.S. Influences of dietary uptake and reactive sulfides on metal bioavailability from aquatic sediments. *Science* **2000**, *287*, 282–284. [[CrossRef](#)] [[PubMed](#)]
37. Hornibrook, E.R.C.; Bowes, H.L.; Culbert, A.; Gallego-Sala, A.V. Methanotrophy potential versus methane supply by pore water diffusion in peatlands. *Biogeosciences* **2009**, *6*, 1491–1504. [[CrossRef](#)]
38. Lerman, A. *Geochemical Processes: Water and Sediment Environments*; John Wiley: New York, NY, USA, 1979; 481p.
39. Rose, C.; Crumpton, W.G. Spatial patterns in dissolved oxygen and methane concentrations in a prairie pothole wetland in Iowa, USA. *Wetlands* **2006**, *26*, 1020–1025. [[CrossRef](#)]
40. Shoemaker, J.K.; Varner, R.K.; Schrag, D.P. Characterization of subsurface methane production and release over 3 years at a New Hampshire wetland. *Geochim. Cosmochim. Acta* **2012**, *91*, 120–139. [[CrossRef](#)]
41. Wang, Y.; Yang, H.; Ye, C.; Chen, X.; Xie, B.; Huan, C.; Zhang, J.; Xu, M. Effects of plant species on soil microbial processes and CH₄ emission from constructed wetlands. *Environ. Pollut.* **2013**, *174*, 273–278. [[CrossRef](#)] [[PubMed](#)]
42. Miao, Y.; Song, C.; Wang, X.; Sun, X.; Meng, H.; Sun, L. Greenhouse gas emissions from different wetlands during the snow-covered season in Northeast China. *Atmos. Environ.* **2012**, *62*, 328–335. [[CrossRef](#)]
43. Aubertin, M.; Aachib, M.; Authier, K. Evaluation of diffusive gas flux through covers with a GCL. *Geotext. Geomembr.* **2000**, *18*, 215–233. [[CrossRef](#)]
44. Rasmussen, H.; Jørgensen, B.B. Microelectrode studies of seasonal oxygen uptake in a coastal sediment: Role of molecular diffusion. *Mar. Ecol. Prog. Ser.* **1992**, *81*, 289–303. [[CrossRef](#)]
45. Yun, J.; Yu, Z.; Li, K.; Zhang, H. Diversity, abundance and vertical distribution of methane-oxidizing bacteria (methanotrophs) in the sediments of the Xianghai wetland, Songnen Plain, northeast China. *J. Soils Sediments* **2013**, *13*, 242–252. [[CrossRef](#)]
46. Liebner, S.; Schwarzenbach, S.P.; Zeyer, J. Methane emissions from an alpine fen in central Switzerland. *Biogeochemistry* **2012**, *109*, 287–299. [[CrossRef](#)]

47. Chmura, G.L.; Kellman, L.; Guntenspergen, G.R. The greenhouse gas flux and potential global warming feedbacks of a northern macrotidal and microtidal salt marsh. *Environ. Res. Lett.* **2011**, *6*, 044016. [[CrossRef](#)]
48. Askaer, L.; Elberling, B.; Glud, R.N.; Kühl, M.; Lauritsen, F.R.; Joensen, H.P. Soil heterogeneity effects on O₂ distribution and CH₄ emissions from wetlands: In situ and mesocosm studies with planar O₂ optodes and membrane inlet mass spectrometry. *Soil Biol. Biochem.* **2010**, *42*, 2254–2265. [[CrossRef](#)]
49. Song, H.; Liu, X. Anthropogenic effects on fluxes of ecosystem respiration and methane in the Yellow River Estuary, China. *Wetlands* **2016**, *36*, 113–123. [[CrossRef](#)]
50. Jerman, V.; Metje, M.; Mandić-Mulec, I.; Frenzel, P. Wetland restoration and methanogenesis: The activity of microbial populations and competition for substrates at different temperatures. *Biogeosciences* **2009**, *6*, 1127–1138. [[CrossRef](#)]
51. Brix, H. Gas exchange through dead culms of reed, *Phragmites australis* (Cav.) Trin. ex Steudel. *Aquat. Bot.* **1989**, *35*, 81–98. [[CrossRef](#)]
52. Holzapfel-Pschorn, A.; Conrad, R.; Seiler, W. Effects of vegetation on the emission of methane from submerged paddy soil. *Plant Soil* **1986**, *92*, 223–233. [[CrossRef](#)]
53. Schütz, H.; Holzapfel-Pschorn, A.; Conrad, R.; Rennenberg, H.; Seiler, W. A 3-year continuous record on the influence of daytime, season, and fertilizer treatment on methane emission rates from an Italian rice paddy. *J. Geophys. Res. Atmos.* **1989**, *94*, 16405–16416. [[CrossRef](#)]
54. Butterbach-Bahl, K.; Papen, H.; Rennenberg, H. Impact of gas transport through rice cultivars on methane emission from rice paddy fields. *Plant Cell Environ.* **1997**, *20*, 1175–1183. [[CrossRef](#)]
55. King, J.Y.; Reeburgh, W.S.; Regli, S.K. Methane emission and transport by arctic sedges in Alaska: Results of a vegetation removal experiment. *J. Geophys. Res. Atmos.* **1998**, *103*, 29083–29092. [[CrossRef](#)]
56. Kelker, D.; Chanton, J. The effect of clipping on methane emissions from *Carex*. *Biogeochemistry* **1997**, *39*, 37–44. [[CrossRef](#)]
57. Green, S.M.; Baird, A.J. A mesocosm study of the role of the sedge *Eriophorum angustifolium* in the efflux of methane—including that due to episodic ebullition—from peatlands. *Plant Soil* **2012**, *351*, 207–218. [[CrossRef](#)]
58. Waddington, J.M.; Roulet, N.T.; Swanson, R.V. Water table control of CH₄ emission enhancement by vascular plants in boreal peatlands. *J. Geophys. Res. Atmos.* **1996**, *101*, 22775–22785. [[CrossRef](#)]
59. Stanley, E.H.; Ward, A.K. Effects of vascular plants on seasonal pore water carbon dynamics in a lotic wetland. *Wetlands* **2010**, *30*, 889–900. [[CrossRef](#)]
60. Martens, C.S.; Albert, D.B.; Alperin, M.J. Biogeochemical processes controlling methane in gassy coastal sediments—Part 1. A model coupling organic matter flux to gas production, oxidation and transport. *Cont. Shelf Res.* **1998**, *18*, 1741–1770. [[CrossRef](#)]
61. Borrel, G.; Jézéquel, D.; Biderre-Petit, C.; Morel-Desrosiers, N.; Morel, J.P.; Peyret, P.; Fonty, G.; Lehours, A.C. Production and consumption of methane in freshwater lake ecosystems. *Res. Microbiol.* **2011**, *162*, 832–847. [[CrossRef](#)] [[PubMed](#)]
62. Frenzel, P.; Thebrath, B.; Conrad, R. Oxidation of methane in the oxic surface layer of a deep lake sediment (Lake Constance). *FEMS Microbiol. Lett.* **1990**, *73*, 149–158. [[CrossRef](#)]
63. Nielsen, L.P.; Christensen, P.B.; Revsbech, N.P.; Sørensen, J. Denitrification and oxygen respiration in biofilms studied with a microsensor for nitrous oxide and oxygen. *Microb. Ecol.* **1990**, *19*, 63–72. [[CrossRef](#)] [[PubMed](#)]
64. Valentine, D.L.; Reeburgh, W.S. New perspectives on anaerobic methane oxidation. *Environ. Microbiol.* **2000**, *2*, 477–484. [[CrossRef](#)] [[PubMed](#)]
65. Caldwell, S.L.; Laidler, J.R.; Brewer, E.A.; Eberly, J.O.; Sandborgh, S.C.; Colwell, F.S. Anaerobic oxidation of methane: Mechanisms, bioenergetics, and the ecology of associated microorganisms. *Environ. Sci. Technol.* **2008**, *42*, 6791–6799. [[CrossRef](#)] [[PubMed](#)]
66. Baird, A.J.; Beckwith, C.W.; Waldron, S.; Waddington, J.M. Ebullition of methane-containing gas bubbles from near-surface Sphagnum peat. *Geophys. Res. Lett.* **2004**, *31*. [[CrossRef](#)]

